Analyst

ROYAL SOCIETY OF CHEMISTRY

MINIREVIEW

View Article Online
View Journal | View Issue

Cite this: *Analyst*, 2025, **150**, 447

High-sensitivity and stability electrochemical sensors for chlorogenic acid detection based on optimally engineered nanomaterials

Lin-Wei Chen, *[a] Nannan Lu [a] and Lei Wang *[b]

Developing cost-effective and efficient analytical methods is essential for detecting chlorogenic acid (CGA), as excessive consumption of CGA, despite its significant antioxidant, anticancer, and anti-inflammatory properties, can cause serious health problems. The remarkable progress and adjustable features of nanomaterials have significantly improved the analytical capabilities of electrochemical sensors for CGA. This review examines the use of optimally engineered nanomaterials in CGA electrochemical sensors, emphasizing the design and modification strategies of various nanomaterials. It starts with an introduction to the basic principles of electrochemical sensors, detailing their components and the analytical methods employed. Subsequently, the review explores how structural and compositional adjustments in electrocatalysts from different nanomaterial categories enhance CGA detection performance. In conclusion, it discusses the challenges and opportunities linked to designing nanomaterials for modified electrodes in CGA sensors. This review seeks to enhance the understanding of the connection between nanomaterial structures and the performance of CGA electrochemical sensors, offering new perspectives for the future design of highly efficient CGA electrochemical sensors.

Received 28th November 2024,
Accepted 5th January 2025

DOI: 10.1039/d4an01483a

rsc.li/analyst

1. Introduction

Chlorogenic acid (CGA) is an important bioactive dietary polyphenol primarily produced by plants. It is widely found in various dietary sources such as coffee beans, potato tubers, sweet potato leaves, eggplants, sunflower seeds, and a variety of other fruits and vegetables.[1–3] Growing research indicates that CGA has significant antioxidant, anticancer, and anti-inflammatory properties, making these health benefits a focal point in recent epidemiological studies.[4,5] CGA is suggested to offer numerous health benefits, including improving conditions such as diabetes,[6] obesity,[7] Alzheimer's disease,[8] stroke,[9] endothelial function, and blood pressure.[10,11] However, some studies have revealed potential side effects, indicating that intake exceeding 7 mg per kg body weight could cause severe conditions like allergic reactions, oxidative stress, vomiting, inflammatory responses, nausea, and dermatitis.[12–14] Thus, developing an accurate, sensitive, and low-cost method for detecting CGA is crucial for ensuring human health.

Currently, various methods for CGA detection have been reported, including liquid chromatography,[15] liquid chromatography-mass spectrometry,[16] fluorescence,[17] ultraviolet and visible spectroscopy,[18] infrared spectroscopy,[19] capillary electrophoresis,[20] and electrochemical analysis techniques.[21] Among these methods, electrochemical analysis techniques that convert chemical information into electrical signals, namely electrochemical sensors, stand out in the detection of CGA. For example, we can estimate the concentration of target molecules by recording the current flow, based on the principle that the electron transfer resulting from the redox reactions at the electrode–electrolyte solution interface is proportional to the concentration of the analyte in the solution.[22] In addition to simplicity, electrochemical analysis methods offer novelty in terms of technology, applications, and performance, compared to traditional analytical methods. These advantages include versatility, speed, on-site applicability, and selectivity. As a result, electrochemical methods hold significant application value in fields such as medical diagnostics, food safety, and environmental protection.[23] However, bare electrodes used in electrochemical analysis often face issues such as narrow linear range, insufficient detection limits, and poor sensitivity.[24] Modifying electrodes is a reliable method to enhance detection performance for target substances, making the development of efficient modified electrodes crucial for CGA detection. Nanomaterials, with their high surface area-to-

[a]*School of Pharmacy, Anhui University of Chinese Medicine, Hefei, 230012, China. E-mail: chenlw@ahtcm.edu.cn*
[b]*School of Chemistry and Chemical Engineering, Yangzhou University, Yangzhou, Jiangsu 225009, China. E-mail: leiwang88@yzu.edu.cn*

volume ratio, excellent electrical conductivity, and unique catalytic properties, enable more effective electron transfer processes and greater surface adsorption of target molecules. Consequently, incorporating nanomaterials into electrochemical sensors can significantly enhance the molecular interactions between the various components of the sensor, thereby substantially improving the overall detection sensitivity of the electrochemical sensor (Fig. 1).[25,26]

This study reviews the application of optimally designed nanomaterials in CGA electrochemical sensors, with a focus on the design and modification strategies of various nanomaterials. It begins with an overview of the fundamental theories of electrochemical sensors, including their composition and the analytical techniques involved. We briefly introduce voltammetry and amperometry, which are commonly used to detect phenolic compounds, as CGA belongs to the class of phenolic compounds. Following this, the study discusses the enhanced detection performance of CGA achieved through structural and component modulation of electrocatalysts from different categories of nanomaterials. Specifically, we begin the discussion by focusing on carbon-based materials from different dimensional perspectives, primarily emphasizing composite materials of carbon with inorganic nanoparticles (such as metals or metal oxides) to highlight the synergistic effects of these composites, which enhance the performance and reliability of the sensors. We then categorize and discuss composite materials based on metal–organic frameworks (MOFs) or oxides as the material center, emphasizing the advantages of the crystal structure of MOFs and oxides, the tunability of their compositions, and their synergistic effects. Additionally, a brief section is devoted to the development of CGA electrochemical sensors using other base electrodes. Finally, it addresses the challenges and possibilities associated with designing nanomaterials for modified electrodes in CGA sensors. This review aims to deepen the understanding of the relationship between the structure of nanomaterials and the performance of CGA electrochemical sensors, providing new insights for the future design of highly efficient CGA electrochemical sensors.

2. Fundamentals of electrochemical sensors

Electrochemical sensors are sophisticated devices that includes an electrochemical transducer, which is capable of harnessing electrochemical reactions, such as oxidation–reduction (redox) reactions, to transform the response generated by the interaction between the target analyte and the sensing element into a measurable electrical signal. The nature of these electrical signals, manifesting as changes in current, voltage, or conductivity, is directly correlated with the concentration of the analyte being detected. As shown in Fig. 2, an electrochemical sensor typically consists of a three-electrode system: a reference electrode (RE), a counter electrode (CE), and a working electrode (WE). The RE provides a stable and known potential as a reference point to accurately measure the potential of the WE. The CE completes the circuit, allowing current to flow through the electrolyte solution. The WE is where electrocatalytic reactions occur, and its materials (solid conductive materials, such as Pt, Au, or carbon) and surface properties significantly affect the sensor's performance. By modifying the WE, such as coating its surface with nanomaterials, we can enhance the electrocatalytic activity.[27] Based on the key parameters (sensitivity, detection limit, dynamic range, selectivity, linearity, response time, and stability) of electrochemical sensors, optimizing conditions can achieve high sensitivity, specificity, and rapid response time for electrochemical sensors, which are of significant value in applications such as environmental monitoring and food safety.

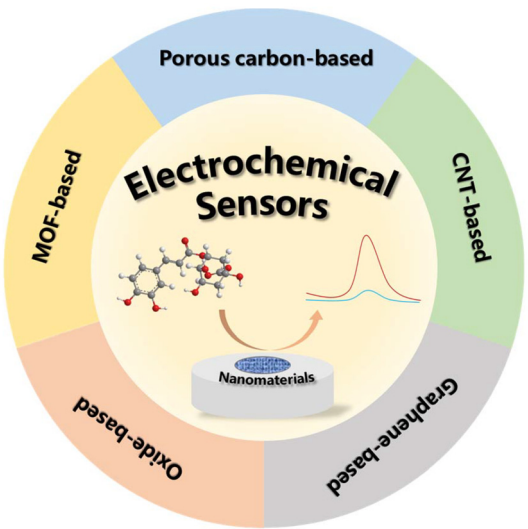

Fig. 1 Illustration of the nanomaterials-based electrochemical sensors for detecting chlorogenic acid.

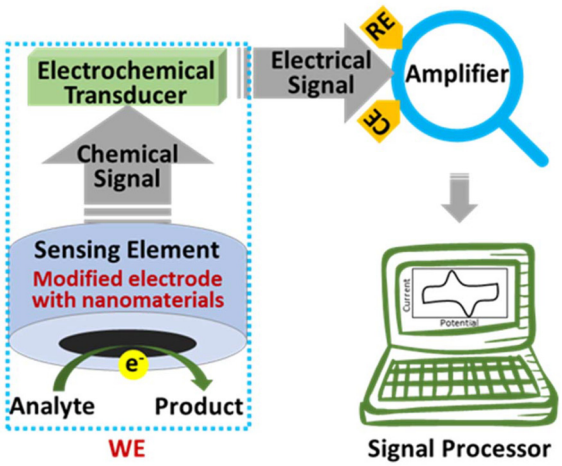

Fig. 2 Schematic diagram of a typical electrochemical sensor.

With the advancement of electrochemical methods in recent years, the construction of electrochemical sensors has facilitated the detection of analytes through measurable data obtained from various electrochemical analytical techniques. These analytical techniques include, but are not limited to, amperometry (based on the generation of measurable current), voltammetry (based on the current–potential curves), potentiometry (based on the generation of measurable or controllable potential), and electrochemical impedance spectroscopy (an electrochemical technique involving the measurement of impedance at the electrode/solution interface). In the analysis of phenolic compounds, the electrochemical techniques commonly employed for detecting phenolic substances, based on the interfacial interactions between phenolic compounds and nanomaterials modifying the WE, mainly include voltammetry and amperometry.[28] Note that the most common and widely used voltammetric techniques, such as cyclic voltammetry (CV) and linear sweep voltammetry (LSV), are extensively employed to study the electrochemical behavior of electroactive molecules, and differential pulse voltammetry (DPV) and square wave voltammetry (SWV), which are classified under pulse voltammetry techniques, are utilized to investigate the redox properties of trace amounts of electroactive compounds. Pulse voltammetry techniques are characterized by their use of short-duration potential or current variations, offering significant advantages over traditional methods. On one hand, they can minimize the impact of charging current, thereby achieving higher sensitivity; on the other hand, they enable more precise analysis of electrode reactions by extracting only the faradaic current, which is directly related to the redox processes of the electroactive species.[29] This makes pulse techniques widely used in the development of electrochemical sensors, especially in applications requiring high sensitivity and high resolution.

3. Electrochemical nanomaterials-based sensors for chlorogenic acid

For over two decades, nanostructured materials, including carbon-based materials, metal–organic frameworks (MOFs), oxides, and more, have provided feasible platforms for electroanalysis due to their unique physical and chemical properties, especially in the design and development of modified electrodes for electrochemical sensing applications.[30] In electrochemical sensors, nanomaterials used to modify the WE surface act as catalysts, facilitating redox processes at the electrode surface.[31] This catalytic activity is crucial for sensor performance, directly impacting the efficiency and effectiveness of the sensing mechanism. Furthermore, the incorporation of nanomaterials into electrochemical sensors offers significant advantages, particularly in terms of enhancing the sensors' stability, sensitivity, and selectivity. This is especially important when the sensors are exposed to common interferences that could otherwise compromise their performance. The ability of nanomaterials to mitigate these interferences ensures that the sensors maintain high levels of accuracy and reliability. Consequently, the introduction of nanomaterials into electrochemical detection has markedly improved the sensing response of electrochemical sensors.

This section covers several important types of nanomaterials and nanocomposites that have been widely used in designing high-performance electrochemical sensors for detecting chlorogenic acid. In addition to reviewing glassy carbon electrodes (GCE) as sensing platforms, some non-traditional sensing platforms, such as carbon papers (CP), screen-printed electrodes (SPE), carbon paste electrodes (CPE), and pencil graphite electrodes (PIGE), 3D printed electrodes (3DE) have also been modified with different nanomaterials. The following content provides a comprehensive overview of advancements in electrochemical sensor technology by analyzing various electrode platforms and their nanomaterial modifications, demonstrating how these innovations enhance the accuracy, sensitivity, and reliability of chlorogenic acid detection. Table 1 summarizes the analytical features of electrochemical sensors constructed based on nanomaterials for detecting CGA.

3.1 Modified GCE with carbon-based nanomaterials

Carbon-based nanomaterials are considered excellent candidates for assembling electrochemical sensors due to their high specific surface area, exceptional electrical conductivity, robust chemical stability, superior mechanical strength, and highly tunable surface characteristics.[58–60] In the realm of chlorogenic acid sensing systems, three primary types of carbon-based nanomaterials have been extensively designed and utilized: three-dimensional (3D) porous carbon-based materials, two-dimensional (2D) graphene-based materials, and one-dimensional (1D) carbon nanotube-based materials. Each of these materials offers unique advantages that enhance the performance of the sensors. To further enhance the stability and electrical properties of electrochemical sensors, as well as to achieve superior electrocatalytic activity for chlorogenic acid detection, carbon materials are often combined with other functional materials. This composite approach typically involves incorporating inorganic nanoparticles, such as metals or metal oxides, rather than merely using carbon materials to modify the electrodes. This strategy leverages the synergistic effects of the combined materials, leading to improved sensor performance and reliability.

In electrochemical sensors, the rapid transport of reactants and products is crucial for improving the sensor's response speed, sensitivity, and stability. 3D porous carbon materials, with their 3D spatial continuity and abundant porous structure, provide channels for the diffusion of reactants and products, reducing the migration distance between them on the electrode surface. This significantly accelerates the transfer rate of reactants and enhances the mass transport process. Moreover, the highly interconnected 3D network provides rapid and continuous electron transport pathways, thereby improving the overall efficiency of the electrochemical reaction. Zhang *et al.*[47] developed a sensing platform for detecting

Table 1 Summary of nanomaterials-based electrochemical sensors for CGA determination

Modification material	Electrode	Detection technique	Linear range (μM)	LOD (μM)	Application	Ref.
Au/PcFe@HZIF-8	GCE	DPV	0.03–500	0.01	Coffee, tea	32
Co–L@RGO	GCE	DPV	0.1–20	7.24×10^{-3}	Honeysuckle	33
mNPC@rGO/$NiFe_2O_4$	GCE	DPV	1×10^{-4}–20	2×10^{-5}	Coffee grounds, eucommia ulmoides, serum	34
Gd_2O_3/W-CNTs	GCE	SWV	2.5×10^{-3}–1.6	1.08×10^{-3}	Coffee	35
Co-MOF/BP-RGO	GCE	DPV	0.001–391	0.014	Coffee, tea	36
Pt@Pd NWs-Hemin-PEI-rGO	GCE	DPV	0.5–4 × 10^{-3}	7.8×10^{-3}	Coffee, soft drink	37
Bi_2CuO_4-KOH	GCE	DPV	0.05–556	4.8×10^{-3}	Coffee, tea, apple, honeysuckle	38
MOF-818@RGO/MWCNTs	GCE	DPV	0.2–50	5.7×10^{-3}	Human serum, human urine	39
NbNPs/CNTs	GCE	SWV	2×10^{-3}–2	8.2×10^{-4}	Coffee, tomato, drinks	40
CuTCPP/pOMC	GCE	Amperometry	0.1–15	0.019	Green coffee bean tablets	41
ZnO@PEDOT:PSS	GCE	DPV	0.03–476.2	0.02	Coffee, soft drinks	42
LGN-MWCNTs-CuONPs	GCE	DPV	5–50	0.0125	Coffee	43
Fe_3O_4@MIL100(Fe)	GCE	DPV	0.1–460	0.05	—	44
TAPB-DMTP-COFs/AuNPs	GCE	DPV	0.01–40	9.5×10^{-3}	Coffee, apple, honeysuckle	45
Graphene	GCE	SW-AdSV	0.014–1.4	3.2×10^{-3}	Vanilla sugar, vanillin enriched instant coffee, cola soft drink	46
Au-POMs-MPC	GCE	DPV	2.28×10^{-3}–3.24	2.15×10^{-3}	Tablets of CGA	47
CS/MWCNTs	GCE	DPV	0.02–225	0.0116	Human serum	48
UiO-66-NH_2/TiO_2	GCE	DPV	0.01–15	7×10^{-3}	Coffee, tea	49
MIS/MWCNTs-VTMS	GCE	DPV	0.08–500	0.032	Coffee, tomato, apple	50
Fe_3O_4/ZnO	GCE	LSV	0.05–1291	5.1×10^{-3}	Coffee, tea	51
DSiFPC	GCE	DPV	0.03–1	6.2×10^{-3}	Lonicera japonica, eucommia ulmoides	52
DSiFPC	SPCE	DPV	0.1–10	0.0358	Lonicera japonica, eucommia ulmoides	52
GPH-GNP	SPCE	CV	0.1–1.2	0.062	nutraceutical products	53
ZIF-67/PEDOT	CP	DPV	0.1–40	3×10^{-3}	Honeysuckle	54
CdSe QD/*meso*-silica/rGO	PIGE	SWV	5.9×10^{-3}–0.52	1.97×10^{-3}	Coffee, tea	55
RTIL/DMC	CPE	SWV	0.02–2.5	0.01	*Echinacea purpurea*, calendula officinalis	56
SACP@Au	3DE	CV	10–400	4.13	Coffee	57

CGA using an electrode modified with 3D macroporous carbon (MPC) composite Au nanoparticles (Au-POMs-MPC/GCE). The detailed design of this platform involves Keggin-type polyoxometalates (POMs), $H_3PW_{12}O_{40}$, to synthesize stable colloidal Au nanoparticles, which were then attached to MPC at mild temperatures (Fig. 3a). The choice of POMs is particularly significant due to their inherent redox and photochemical properties, which enable them to participate in reversible multi-electron redox transitions. This characteristic is crucial for the effective functioning of the sensor. On the other hand, the MPC exhibits a unique interconnected macroporous nanostructure (~110 nm pore size), high specific surface area, large pore volume, excellent conductivity, good thermal stability, and chemical inertness, providing a platform for uniformly dispersed Au nanoparticles (Fig. 3b). Note that, compared to larger particles, high-dispersion metal nanoparticles are more desirable in applications such as catalysis, electrochemical sensing, and energy storage. This is because they provide more active sites, reduce metal consumption, and enhance electrochemical performance.[61] The favorable chemical and electronic interactions between MPC and nanoparticles resulted in synergistic enhancement of electrocatalytic activity of the sensor. To investigate the electrochemical behavior of CGA on the Au-POMs-MPC/GCE, CV was employed at various scan rates. The results revealed a linear increase in the electrochemical response with the square root of the scan rate (ν) over the range of 5 to 300 mV s^{-1}, indicating diffusion-controlled kinetics. A series of DPV curves obtained from different concentrations of CGA (Fig. 3c) indicated that the CGA sensor achieves a linear detection range from 2.28 nM to 3.24 μM (R = 0.9963), a sensitivity of 30 554.71 μA mM^{-1}, and a calculated detection limit of 2.15 nM. This highly effective method has been successfully applied to the determination of CGA in tablet formulations, showcasing its practical applicability and reliability.

Recently, biomass-derived porous carbon has gained significant attention due to its wide availability of raw materials, low production cost, and high density of surface functional groups that facilitate easy functionalization. These characteristics collectively contribute to its increasing popularity in sensor applications.[62,63] Jiang *et al.*[52] synthesized hierarchical porous carbon using a soft–hard dual template method with silica colloids, various surfactants, and plant-derived tannic acid as the carbon source (Fig. 3d). Among them, the DSiFPC material, prepared with triblock copolymer Pluronic F127, exhibited micropores, mesopores, and macropores, forming a unique hierarchical porous structure (observed by TEM). It showed high specific surface area and pore volume (measured by BET). Macropores and mesopores aid mass transfer, while micropores enhance surface area and pore volume. Moreover, the use of tannic acid as the carbon source results in a porous carbon material with a surface rich in oxygen groups (confirmed by XPS), exposing numerous active sites that enhance the electrochemical sensing performance of DSiFPC. DSiFPC modified GCE for detecting CGA in dried honeysuckle flowers and SPCE for on-site detection in fresh Eucommia leaves. The

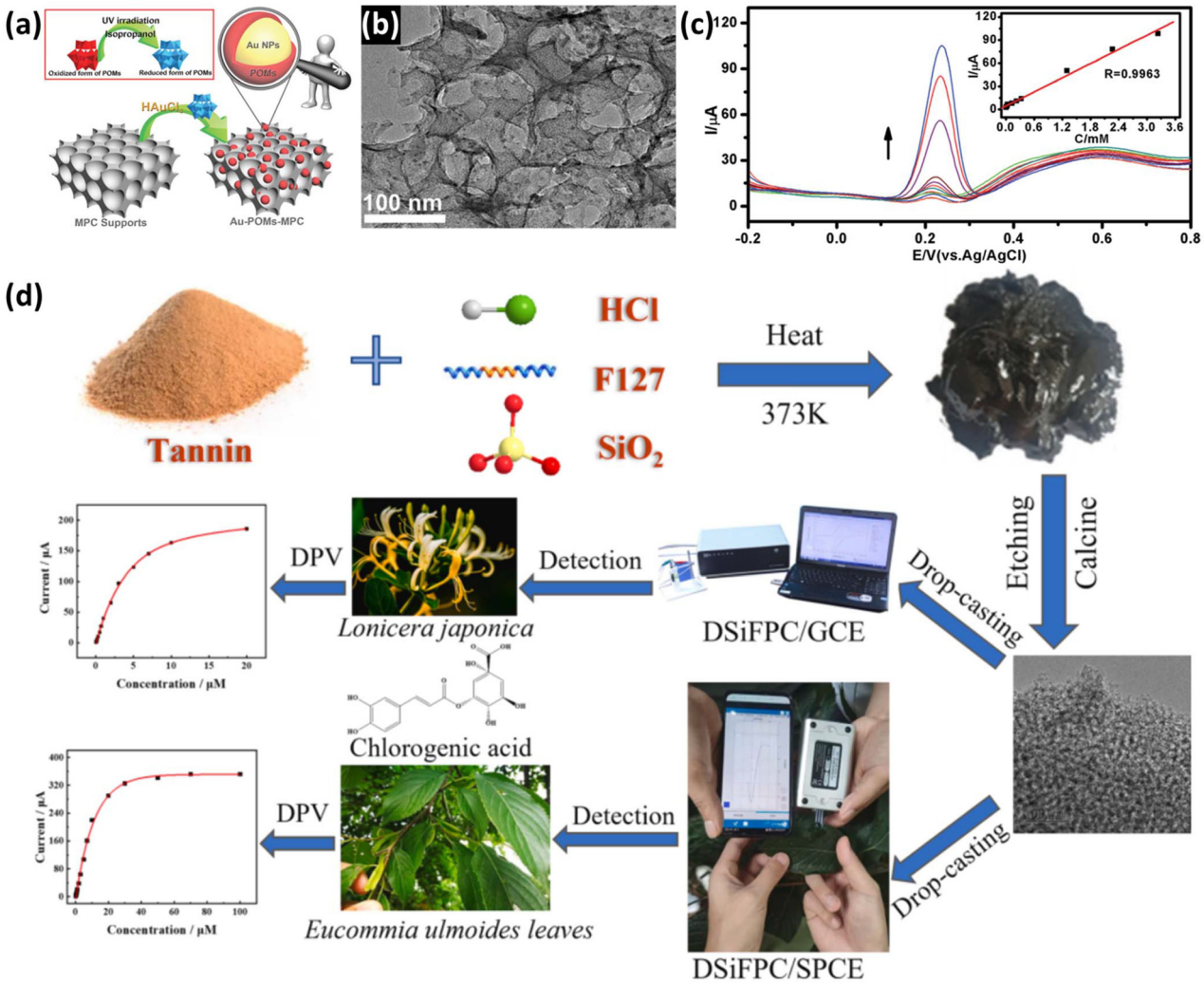

Fig. 3 (a) Schematic representation of the preparation of Au-POMs-MPC. (b) TEM images depicting the structure of Au-POMs-MPC. (c) DPV curves of CGA in PBS (0.1 M, pH 7.0) using the Au-POMs-MPC/GCE. The inset in (c) shows the linear relationship between the current response and varying concentrations of CGA. (a–c) Reprinted by permission from ref. 47. Copyright, 2017, Royal Society of Chemistry. (d) Electrochemical detection of CGA in both the flowers of Lonicera japonica and the fresh leaves of Eucommia ulmoides was performed using a smartphone-operated wireless portable sensor based on a DSiFPC/SPCE three-electrode system. This modern sensor was compared with a traditional sensor based on a DSiFPC/GCE system. Reprinted by permission from ref. 52. Copyright, 2024, Elsevier.

peak current values for the cathodic and anodic processes show a linear relationship with the square root of ν, indicating a diffusion-controlled electrochemical process in the redox of CGA. DSiFPC/GCE showed good stability and anti-interference in CGA detection, with a linear range of 0.03–1 μM and a detection limit of 6.2 nM. The traditional sensor based on DSiFPC/GCE successfully achieved electrochemical detection of CGA in actual honeysuckle samples, an ingredient commonly used in herbal tea. Additionally, a smartphone-operated wireless portable sensor with DSiFPC/SPCE enabled low-cost, rapid, on-site CGA detection in Eucommia leaves, showing good recovery. Experimental results indicated that the smartphone-operated wireless portable electrochemical sensor could directly perform *in situ* detection of CGA on fresh Eucommia leaves.

Graphene, a quintessential two-dimensional nanomaterial, is composed of a single layer of sp^2 hybridized carbon atoms arranged in a honeycomb lattice. This atomic-thick planar structure endows graphene with exceptional physicochemical and electrical properties.[64] However, in practical electrochemical detection, reduced graphene oxide (rGO) is often preferred. rGO is produced through the oxidation and subsequent reduction of graphene, a process that introduces additional defects and hydrophilic functional groups. These modifications enhance the electrochemical activity of the material, which is crucial for effective sensor performance. The reduction step is particularly important as oxidized graphene inherently suffers from low electrical conductivity.[65] In addition to having excellent electrical conductivity, large specific surface area, and ease of functionalization, rGO has a

hexagonal ring structure that can bind to the porphyrin ring of hemin *via* π bonds, making it an ideal material for supporting hemin. As shown in Fig. 4a and b, Li *et al.*[37] used hemin-functionalized polyethyleneimine (PEI)-terminated rGO nanosheets as a matrix to load Pt nanoparticles-encapsulated Pd nanowires, forming Pt@Pd NWs-Hemin-PEI-rGO nanohybrids. The PEI, rich in amino groups, effectively enhanced the dispersion of rGO, prevented the self-destruction of hemin, and provided numerous binding sites for Pt@Pd NWs. The interwoven network of Pt@Pd NWs and hemin gave the nanohybrids a large electrochemically active surface area for CGA detection, significantly accelerating electron transfer during the detection process. CV curves at different scan rates showed that the cathodic and anodic peak currents have a good linear relationship with the square root of the scan rate in the range of 10 to 100 mV s^{-1} (Fig. 4c), indicating that the overall reaction kinetics are diffusion-controlled. DPV detection results (Fig. 4d) showed a detection limit of 7.8 nM, a linear range from 0.5 μM to 4 mM, and a sensitivity of 651.523 μA μM^{-1} cm^{-2}, demonstrating excellent trace-level detection capability.

Carbon nanotubes (CNTs), with their unique 1D hollow cylindrical structure, offer additional benefits. This structure is highly tunable in terms of length and diameter, allowing for specific customization based on the application requirements.[66] Multi-walled carbon nanotubes (MWCNTs), which consist of multiple concentric graphene layers, can have diameters reaching up to 100 nm. Furthermore, MWCNTs are known for their high adhesiveness, excellent film-forming capabilities, and biocompatibility. According to reported literature, the research focus on carbon nanotubes in chlorogenic acid sensors is primarily on MWCNTs, likely due to their relatively simple fabrication process, higher yield, and lower cost compared to single-walled carbon nanotubes (SWCNTs), making them more feasible for large-scale industrial applications. For example, by grafting vinyltrimethoxysilane (VTMS) onto MWCNTs and covering them with a molecularly imprinted siloxane (MIS) film prepared through a sol–gel process, an imprinted sensor for detecting CGA was developed.[50] This electrochemical sensor exhibited a linear response over a concentration range from 0.08 μM to 500 μM,

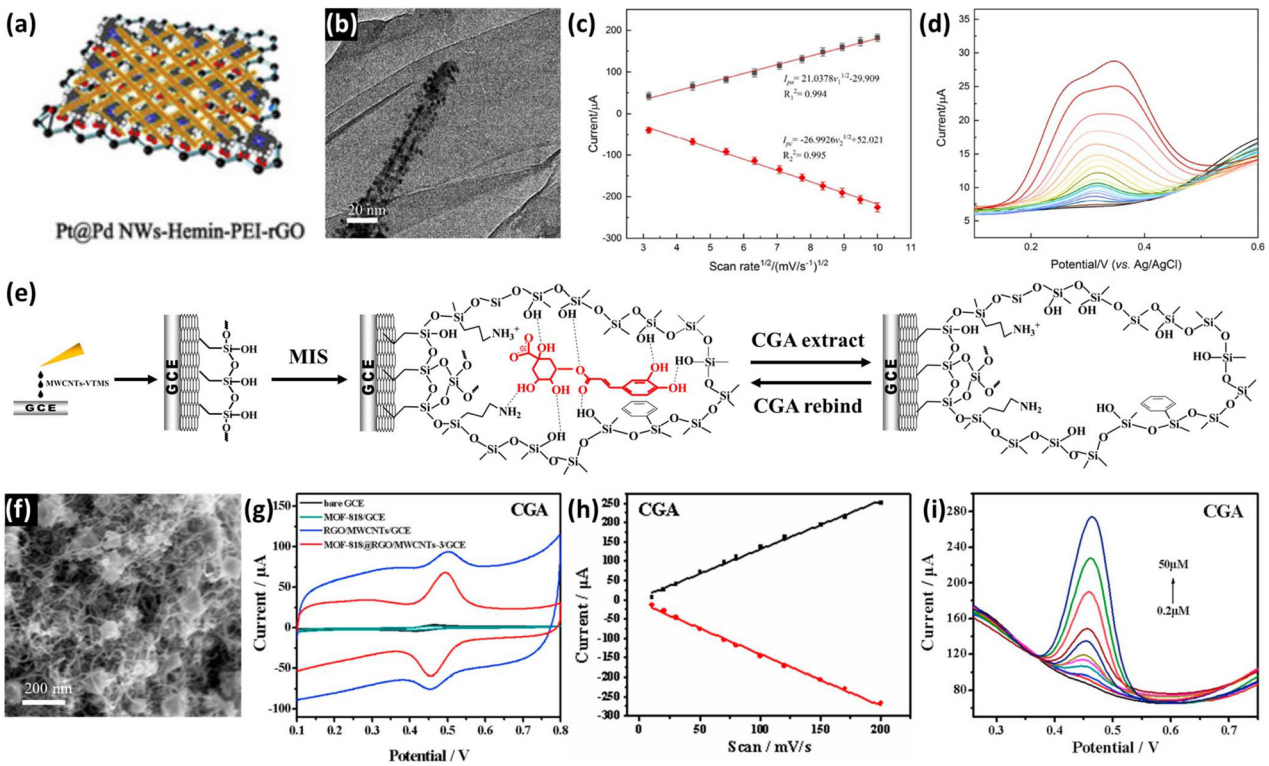

Fig. 4 (a) Schematic diagram and (b) TEM image of Pt@Pd NWs-Hemin-PEI-rGO. (c) Linear relationship obtained for the peak current *vs.* square root of the scan rate. (d) DPV curves of the Pt@Pd NWs-Hemin-PEI-rGO/GCE in PBS buffer solution (pH 4) containing various concentrations of CGA. (a–d) Reprinted by permission from ref. 37. Copyright, 2022, American Chemical Society. (e) Schematic representation for the preparation of MIS/MWCNTs-VTMS/GCE. A homogeneous sol, referred to as MIS, was obtained by stirring a mixture of tetraethoxysilane, phenyltriethoxysilane, (3-aminopropyl)trimethoxysilane, and 2-ethoxyethanol for 10 minutes, followed by the addition of HCl and H_2O and stirring at room temperature. Reprinted by permission from ref. 50. Copyright, 2016, Elsevier. (f) SEM image of MOF-818@RGO/MWCNTs. (g) CV curves of 0.2 mM CGA in 0.1 M PBS (pH = 3.0) at bare GCE, MOF-818/GCE, RGO/MWCNTs/GCE, MOF-818@RGO/MWCNTs-3/GCE. Scan rate: 50 mV s^{-1}. (h) Linear relationships between peak current of CGA with scan rate. (i) DPV curves of different concentration CGA at MOF-818@RGO/MWCNTs-3/GCE 0.1 M PBS (pH = 3.0). (f–i) Reprinted by permission from ref. 39. Copyright, 2020, Elsevier.

with a detection limit of 0.032 μM. In this system, the MWCNTs imparted exceptional sensitivity to the electrode due to their excellent electrical conductivity, high surface area-to-volume ratio, and extreme sensitivity of surface atoms.

The hybridization of CNTs and rGO combines the advantages of 1D and 2D carbon materials, effectively preventing graphene restacking and creating more defects, facilitating electron transfer.[67,68] When rGO/MWCNTs are combined with MOFs, they prevent MOF-818 aggregation, exposing more active sites and improving overall charge transfer. Yan *et al.*[39] synthesized a novel bimetallic MOF-818@rGO/MWCNTs composite using a simple solvothermal method. The rGO/MWCNTs framework, with MWCNTs filling the spaces between the rGO sheets, ensures close contact between the two phases, uniformly dispersing MOF-818 crystals (Fig. 4f). Compared to the bare GCE and other single-component modified GCEs, the MOF-818@rGO/MWCNTs-3/GCE exhibits the best electrochemical response to CGA, attributed to the synergistic amplification effect of MOF-818 and rGO/MWCNTs (Fig. 4g). As shown in Fig. 4h, both oxidation peak current (I_{pa}) and reduction peak current (I_{pc}) increase linearly with the scan rate from 10 to 200 mV s^{-1}, indicating the redox of CGA on MOF-818@rGO/MWCNTs-3/GCE is an adsorption-controlled process. This sensor shows an excellent detection limit for CGA as low as 5.7 nM, with outstanding sensitivity of 12.50 μA Mm^{-1} in the ranges of 0.1–3 μM and 3–20 μM (Fig. 4i). The excellent electrochemical performance of the sensor in detecting CGA is also attributed to the coupling effect of Cu and Zr, which provides more active sites for the bimetallic MOF.[69] The application of MOF-based nanomaterials in CGA electrochemical sensors will be highlighted next.

In summary, carbon-based materials in electrochemical sensors exhibit outstanding performance in enhancing reactant transport, electronic conductivity, sensitivity, stability, and anti-interference capability. However, these materials often face challenges in ensuring consistent pore structure or surface defects across different batches, which may affect the material's uniformity and stability, potentially leading to performance fluctuations.

3.2 Modified GCE with MOF-based nanomaterials

Metal–organic frameworks (MOFs) are nanoporous crystalline materials formed by the coordination bonds between inorganic metal ions and organic ligands. They are self-assembled using metal ion precursors (*e.g.*, nitrates, sulfates) or organic ligands (*e.g.*, carboxylates, azoles) through hydrothermal, microwave, ultrasonic, electrochemical, and diffusion methods.[70] MOFs feature highly tunable pore structures, topologies, cavity structures, high surface areas, and open metal sites, enabling them to selectively absorb, retain, and release molecules, enhancing electrochemical sensor detection limits.[71,72] Additionally, catalytic sites within the ligands and open metal sites in MOFs can improve the selectivity of electrochemical reactions. However, MOFs face poor conductivity and stability, requiring composite materials for better conductivity and performance. For CGA electrochemical sensors, MOF-based nanomaterials combined with carbon materials or oxides can achieve synergistic effects, like the aforementioned MOF-818@RGO/MWCNTs composite.

Zhao *et al.*[33] constructed a novel $[Co_2LCl_4]\cdot 2DMF$ (Co–L) MOF under solvothermal conditions using a functionalized thiacalix[4]arene ligand and Co(II) ions. Subsequently, they combined Co–L with rGO, MWCNT, and mesoporous carbon (MC) to create a series of composite materials, with electrochemical testing identifying Co–L@RGO(1 : 1) as the optimal electrocatalyst for CGA detection. Although MC has the largest specific surface area, its numerous channels hinder the detachment of the CGA oxidation product (Ox-CGA), limiting its catalytic efficiency. Meanwhile, rGO, with a larger specific surface area than MWCNT and functional groups capable of hydrogen bonding with Ox-CGA, exhibits stronger binding with Ox-CGA, resulting in higher peak current responses for Co–L@RGO(1 : 1). The electrocatalytic mechanism of this composite material is as follows: CGA is adsorbed by Co–L, loses electrons, and is oxidized to Ox-CGA. The lost electrons are captured by rGO and transferred to the GCE. Simultaneously, Ox-CGA is also captured by rGO and then diffuses into the solution (Fig. 5a). The CV at different scan rates for 10 μM CGA on Co–L@RGO(1 : 1)/GCE showed that the redox peak current is proportional to the ν, indicating that the redox process of CGA on Co–L@RGO(1 : 1)/GCE is adsorption-controlled (Fig. 5b).

Due to the synergistic effect of Co–L and RGO, the Co–L@RGO(1 : 1)/GCE electrode exhibits a low detection limit of 7.24 nM for CGA concentrations ranging from 0.1 to 20 μM.

Doping graphene with heteroatoms (such as B, N, P, and S) significantly alters its structure and electronic properties. This alteration increases the number of electrochemically active sites and generates more charged sites, facilitating the adsorption and activation of analytes in electrochemical sensors.[73,74] Mariyappan *et al.*[36] developed an advanced electrochemical sensor designed to detect CGA by utilizing a cobalt zeolitic imidazolate framework (Co-MOF) combined with B and P co-doped rGO (BP-rGO) nanocomposite (Fig. 5a). Notably, the Co-MOF/BP-rGO/GCE exhibited the lowest charge transfer resistance (R_{ct}) among the tested materials, indicating that the electron-deficient B and electron-rich P dopants effectively activate adjacent carbon atoms and disrupt the electrical neutrality of the sp^2-bonded carbon system in rGO. Consequently, this disruption creates additional charged sites, enhancing the conductivity of the Co-MOF. Furthermore, the oxidation peak current of CGA exhibited a linear relationship with the scan rate, suggesting that the electrocatalytic redox reaction of CGA on the Co-MOF/BP-rGO nanocomposite is an adsorption-controlled process (Fig. 5b). As depicted in Fig. 5c, the Co-MOF/BP-RGO/GCE displayed a wide linear range (0.001–391 μM), exceptional sensitivity (1.56619 μA μM^{-1} cm^{-2}), and a low detection limit (0.014 μM) under optimized conditions, along with strong long-term stability.

Directly compositing MOFs and oxides, such as preparing MOFs/titanium dioxide ($UiO\text{-}66\text{-}NH_2/TiO_2$) nanocomposites through a simple hydrothermal reaction (Fig. 6a), exhibits

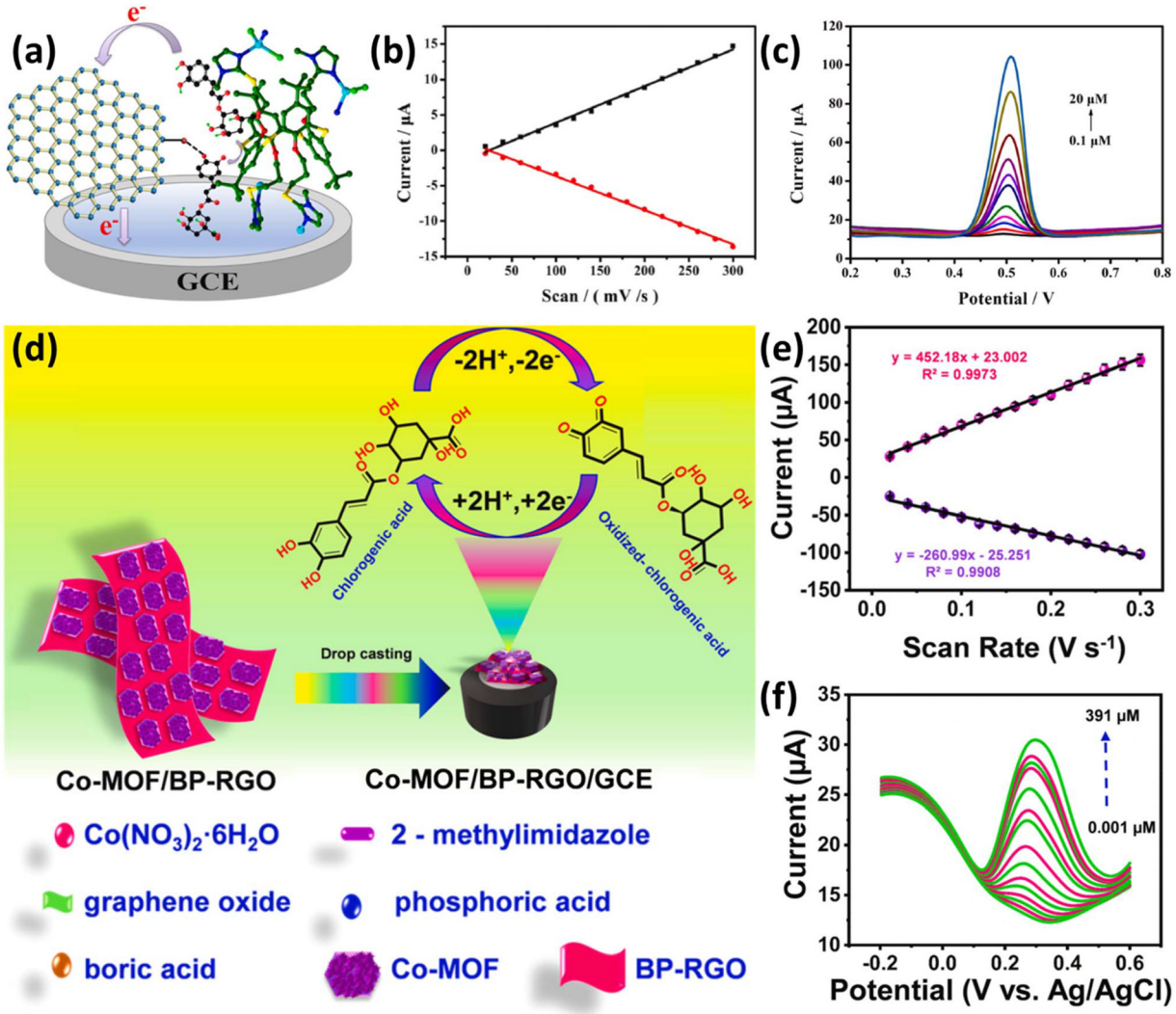

Fig. 5 (a) Electrocatalytic process of Co–L/RGO(1 : 1) towards CGA. (b) Linear relationships between scan rates and peak currents. (c) DPV responses of CGA on the Co–L@RGO(1 : 1)/GCE. (a–c) Reprinted by permission from ref. 33. Copyright, 2023, Elsevier. (d) Illustrates the hydrothermal synthesis of Co-MOF/BP-RGO. (e) The plot illustrating the dependence of anodic and cathodic peak currents on scan rates. (f) DPV current responses for the Co-MOF/BP-RGO/GCE with different concentration additions of CGA in the 0.1 M PBS (pH 7.0). (d–f) Reprinted by permission from ref. 36. Copyright, 2022, Elsevier.

excellent electrocatalytic activity for the oxidation of CGA due to the synergistic effect of UiO-66-NH_2 and TiO_2.[49] The electrode process of CGA on UiO-66-NH_2/TiO_2/GCE is diffusion-controlled (Fig. 6b), and the sensor can detect CGA in the range of 0.01–15 μM, with a detection limit of 7 nM (Fig. 6c). To enhance conductivity and stability by integrating MOFs and metal oxides, one effective method is to prepare core/shell structured composites. Chen *et al.*[44] combined Fe_3O_4 and MIL-100(Fe) to form the magnetic core–shell composite Fe_3O_4@MIL-100(Fe) (Fig. 6a). Adding 200 μM of CGA in blank PBS resulted in a peak current at Fe_3O_4@MIL-100(Fe)/GCE that was about five times higher than at the bare GCE. This improvement is due to the abundant active sites of Fe_3O_4 and MIL-100(Fe), and the MIL-100(Fe) shell preventing Fe_3O_4 aggregation. The peak currents increased with the scanning rate (0.02 to 0.5 V s^{-1}), indicating that the electrochemical process of CGA on Fe_3O_4@MIL-100(Fe)/GCE is a diffusion-controlled process (Fig. 6b). By studying the effect of shell thickness on electrochemical performance, it was found that optimal shell thickness was found to be 10 self-assembly cycles, balancing active site availability and electron transfer efficiency. Under optimal conditions, this electrochemical sensor could quantitatively detect CGA in the range of 0.1–460 μM, with a detection limit as low as 0.05 μM (Fig. 6c).

In summary, MOFs with highly tunable pore structures, high surface areas, and open metal sites demonstrate excellent performance in enhancing the sensitivity, selectivity, and stability of electrochemical sensors. However, to fully leverage these advantages, the issue of poor conductivity in MOFs must be addressed. Therefore, they are often combined with other

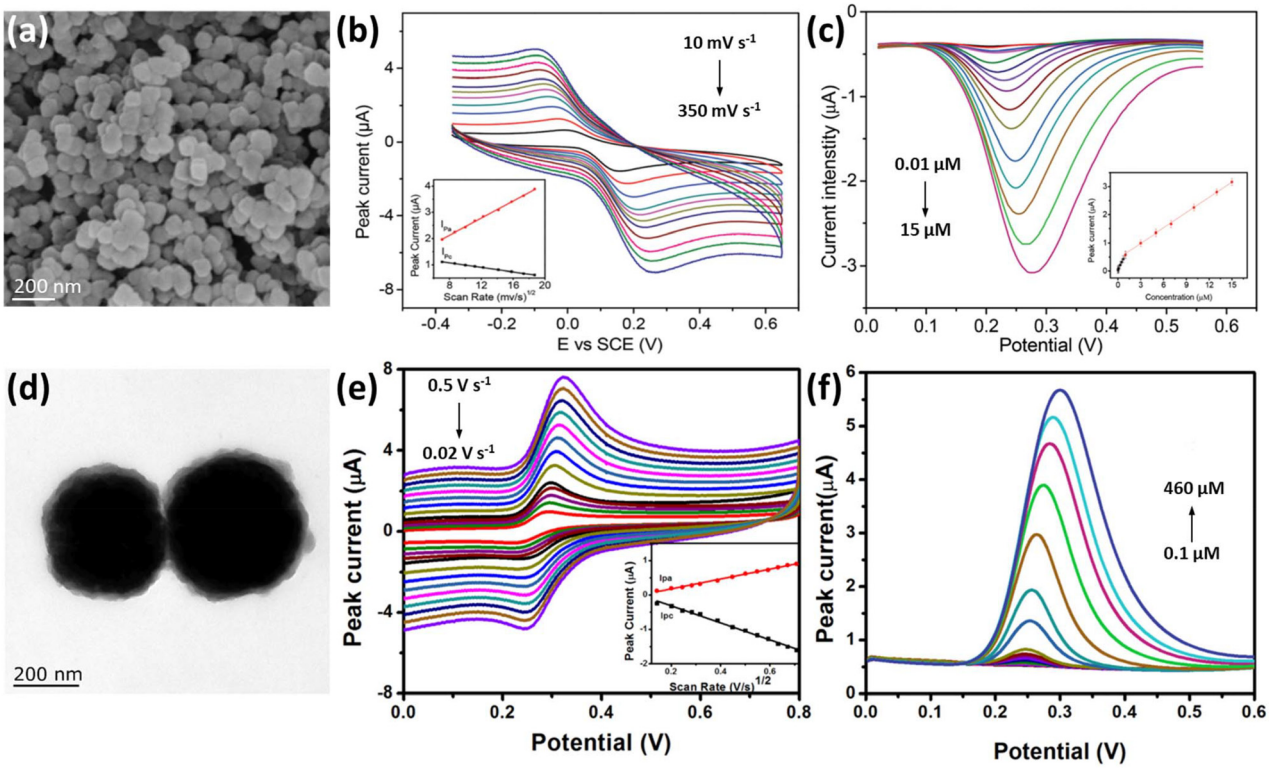

Fig. 6 (a) SEM image of UiO-66-NH_2/TiO_2. (b) CV of CGA at the UiO-66-NH_2/TiO_2/GCE in 0.1 M PBS (pH 6.0) at different scan rates. Inset: The corresponding calibration plot obtained for the square root of the scan rate *vs.* the oxidation peak current. (c) DPV at UiO-66-NH_2/TiO_2/GCE for different concentrations of CGA in pH 6.0 PBS. The inset shows the relationship between the peak current and the CGA concentration (a–c) Reprinted by permission from ref. 49. Copyright, 2016, Royal Society of Chemistry. (d) TEM image of Fe_3O_4@MIL-100(Fe) core–shell magnetic microspheres with ten assembly cycles. (e) CVs of CGA at Fe_3O_4@MIL-100(Fe)/GCE in 0.1 M PBS at various scan rates. Insert: The picture of oxidation/reduction peak current *vs.* square root of scan rate. (f) CV of CGA at the Fe_3O_4@MIL-100(Fe)/GCE, Fe_3O_4/GCE, bare GCE and MIL-100(Fe)/GCE in 0.1 M PBS (pH 6.0) with 200 μM CGA at the scan rate of 0.1 V s^{-1}. Insert: CV of CGA at the Fe_3O_4@MIL-100(Fe)/GCE in 0.1 M PBS (pH 6.0) without CGA. (d–f) Reprinted by permission from ref. 44. Copyright, 2019, Elsevier.

conductive materials (such as graphene or carbon nanotubes) to further enhance their potential for application in electrochemical sensors.

3.3 Modified GCE with oxide-based nanomaterials

In fact, the aforementioned composite systems of MOFs and oxides can also be classified under the category of oxide-based nanomaterials. Here, this discussion focuses on the application of single metal oxide-based and bimetallic oxide-based nanomaterials in the electrochemical detection of CGA. Manivannan *et al.*[42] synthesized flower-like structured ZnO using a one-pot method and coated it with poly(3,4-ethylenedioxythiophene):poly(styrene sulfonate) (PEDOT:PSS) polymer. The synthesized ZnO@PEDOT:PSS modified GCE exhibited a wide linear range and high sensitivity for CGA oxidation, with a detection limit of 0.03–476.2 μM, 29.38 μA μM^{-1} cm^{-2}, 0.02 μM, respectively. Bimetallic oxides, formed by combining two different metals with oxygen, exhibit higher electrochemical activity and stability than single-component nanomaterials due to multivalent cations, unique crystal structures, and tunable compositions.[75,76] For instance, Ganesamurthi *et al.*[51] synthesized Fe_3O_4/ZnO *via* a one-step hydrothermal method, resulting in a modified GCE with a wider linear range (0.05–1291 μM) for CGA detection, a nanomolar detection limit of 5.1 nM, and a sensitivity of 0.05 μA μM^{-1} cm^{-2}. Jesu Amalraj *et al.*[38] synthesized Bi_2CuO_4 with various morphologies using a simple hydrothermal synthesis method. Among all the modified electrode materials, Bi_2CuO_4-KOH/GCE exhibited excellent CGA redox performance due to reduced grain size, increased active surface area, and morphological effects induced by viscosity effects. Using DPV, the Bi_2CuO_4-KOH/GCE demonstrated outstanding electroanalytical performance for CGA, including a wide linear range (0.05–556 μM) and nanomolar-level detection (4.8 nM), with an oxidation sensitivity of up to 0.22 μA μM^{-1} cm^{-2}.

However, both single metal and bimetallic oxides often suffer from weak conductivity and limited exposure of active sites.[77] To mitigate these issues, combining bimetallic oxides with carbon-based materials can enhance conductivity and electrocatalytic activity. For example, Yang *et al.*[34] developed a 2D mesoporous nitrogen-doped carbon/graphene composite (mNPC@rGO/$NiFe_2O_4$) loaded with bimetallic oxide nanospheres by combining the advantages of layered mesoporous and spherical structures (Fig. 7a). The rough surface of

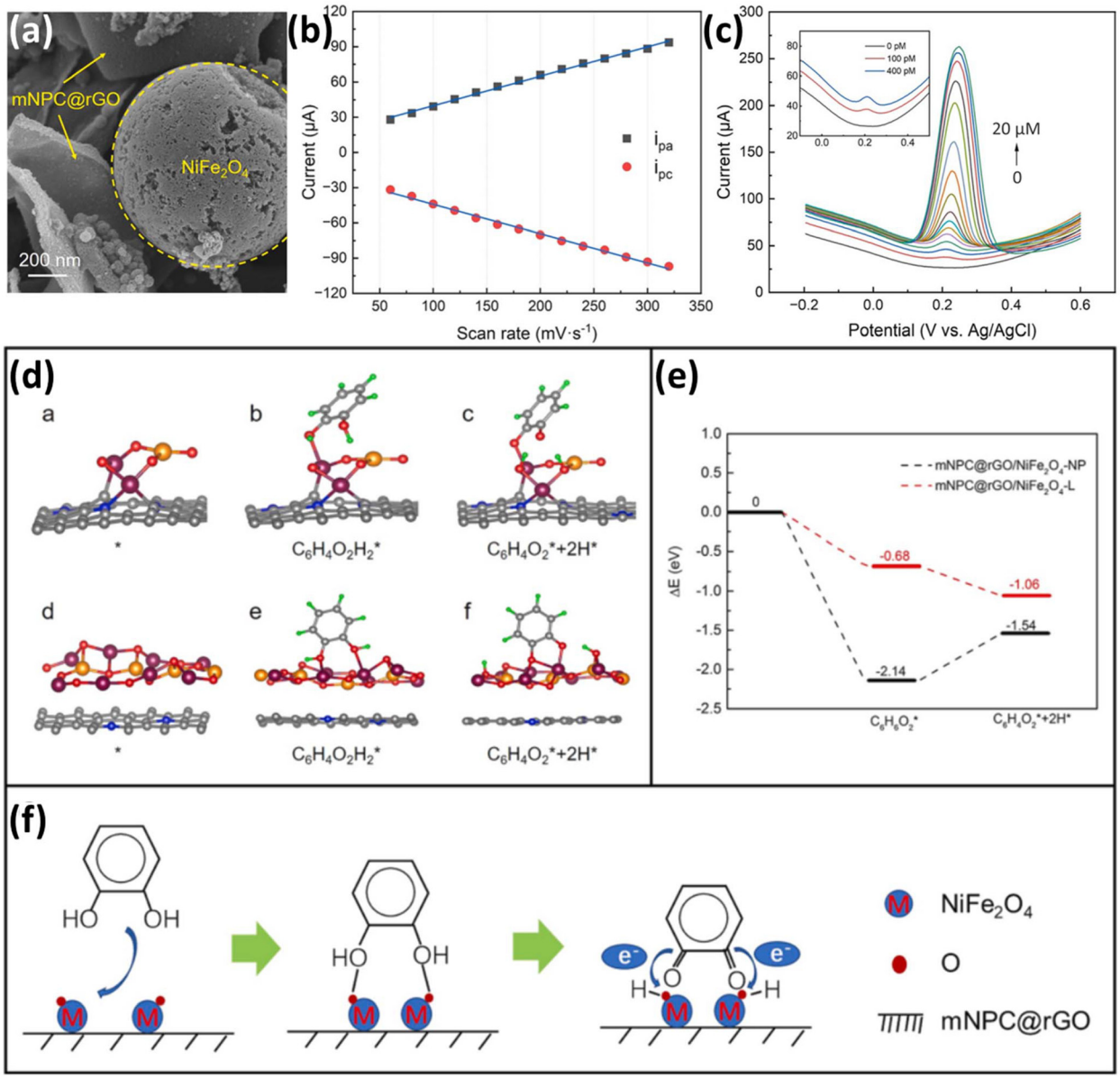

Fig. 7 (a) SEM image of mNPC@rGO/$NiFe_2O_4$. (b) The dependence of redox current on the scan rate. (c) DPVs of CGA quantitative analysis on mNPC@rGO/$NiFe_2O_4$/GCE. Reprinted by permission from ref. 34. Copyright, 2023, Elsevier.

$NiFe_2O_4$ nanospheres ensures sufficient active site exposure and enhances adsorption performance. Additionally, the multivalence of metal elements in $NiFe_2O_4$ promotes redox reactions, and the composite structure prevents interlayer stacking of mNPC@rGO. Fig. 7b shows that the electrode surface is adsorption-controlled, and the sensor constructed with mNPC@rGO/$NiFe_2O_4$/GCE has an impressive sensing capability with a wide linear range of 0.0001–20 μM and a detection limit of 0.02 nM (Fig. 7c). To elucidate the electrocatalytic process of mNPC@rGO/$NiFe_2O_4$ on CGA, the underlying performance enhancements were theoretically investigated by examining the CGA molecule on the mNPC@rGO/$NiFe_2O_4$ surface (Fig. 7d–f). DFT calculations indicated the optimized structure of intermediates on the mNPC@rGO/$NiFe_2O_4$ surface, identifying exposed Fe sites in the $NiFe_2O_4$ unit as active sites. The modification of mNPC@rGO with $NiFe_2O_4$ not only creates Fe sites with better catalytic activity but also optimizes intermediate adsorption by adjusting the electronic structure, thereby enhancing catalytic performance for CGA.

In conclusion, multimetallic oxides, owing to their diverse composition and adjustable structural properties, demonstrate superior electrochemical activity, stability, and conductivity relative to monometallic oxides. However, to further optimize their conductivity and increase the accessibility of active sites, it remains essential to integrate them with conductive materials that can compensate for these shortcomings.

3.4 Modified other signal transducers with nanomaterials

Beyond the prevalent use of GCE as a signal transducer, researchers have explored various other base electrodes such as CP, PIGE, CPE, SPCE and 3DE in the development of electrochemical sensors for CGA. Several typical examples are worth sharing. Ma *et al.*[54] developed an electrode based on a ZIF-67/PEDOT nanocomposite modified CP, which features abundant solution diffusion channels, enhancing electron transfer efficiency. Under optimized conditions, the sensor demonstrated a low detection limit (0.003 μM) and a wide linear range (0.1–40 μM). Jency Feminus *et al.*[55] used a stepwise electrodeposition method to prepare a CdSe QD/mesoporous silica/rGO composite modified PIGE. Under optimized experimental conditions, the sensor exhibited a low detection limit (1.97 nM) and a wide linear range (5.90–523.61 nM). Mohammadi *et al.*[56] developed a CPE electrode modified with highly defective mesoporous carbon (DMC) and room temperature ionic liquid 1-butyl-3-methylimidazolium hexafluorophosphate (BMIM.PF6). The optimized sensor exhibited a linear response range of 0.02 to 2.5 μM and a detection limit of 0.01 μM. Munteanu *et al.* used graphene and Au nanoparticles to modify SPCE, achieving excellent sensitivity (0.062 μM) and a very low detection limit for CGA. 3D printing technology has become an effective tool for the preparation of 3D-printed electrodes. Liao *et al.*[57] modified 3DEs with gold nanoparticles and a poly(3,4-ethylenedioxythiophene):poly (styrene sulfonate) (PEDOT:PSS) composite to construct a novel electrode (SACP@Au@3DE). This electrode exhibited significant electrochemical performance, high sensitivity, and a wide linear response range in CGA detection.

4. Summary and outlook

Nanomaterials have been extensively leveraged in the development of electrochemical sensors for the detection of CGA due to their distinct characteristics, including large specific surface area, excellent catalytic activity, and high electrical conductivity. These unique properties make nanomaterials particularly effective for analysing CGA content in a variety of natural sources such as coffee, tea, fruits, and vegetables. This review delves into the latest advancements in electrochemical CGA sensors that utilize nanomaterials, highlighting that the analytical performance of these sensors is predominantly influenced by the modification of electrodes with nanomaterials. These advanced sensors are noted for their low detection limits, reaching down to nanomolar levels, broad linear analytical ranges, and minimal interference from other substances.

This review systematically summarizes that among the various nanomaterials widely studied as traditional electrode modifiers for CGA detection, carbon-based materials and MOF-based materials have garnered significant attention due to their outstanding redox catalytic activity for CGA. Carbon-based materials, with their high surface-to-volume ratio and numerous active adsorption sites, enhance electrocatalytic performance, making sensors more sensitive to CGA. MOFs, with highly tunable pores, cavity structures, high specific surface area, and open metal sites, can selectively adsorb, retain, and release molecules, thereby improving the detection limits of electrochemical sensors. Furthermore, composite nanomaterials, as opposed to single nanomaterials, facilitate catalytic reactions with target analytes and are highly effective for achieving long-term stability. Thus, to enhance the performance of CGA detection, it is crucial to strategically optimize the structure and composition of various types of nanomaterials. Achieving a high density of catalytic active sites can be accomplished by fine-tuning the size and morphology of nanoparticles to maximize the specific surface area. Furthermore, to improve the overall performance of CGA electrochemical sensors, including sensitivity, selectivity, stability, and response time, it is a wise strategy to combine materials with complementary properties. This approach harnesses the synergistic advantages of each component, offering performance benefits that cannot be achieved by a single material alone.

While most electrochemical sensors exhibit very good selectivity and sensitivity for detecting CGA without the need for sample preparation, many nanomaterial-based CGA sensors are limited by their time-consuming synthesis processes, high costs for mass production, and the toxicity of different types of nanomaterials to humans and the environment. Therefore, introducing nanomaterials with good analytical performance while replacing synthesis with green, inexpensive, scalable, and less time-consuming procedures remains challenging. In addition to the synthesis of nanomaterials and the raw materials, consistency problems related to electrochemical response strength, selectivity, stability, and other factors of nanomaterial-based CGA sensors cannot be ignored. As a result, the consistency of nanomaterial synthesis and the uniformity of electrode modification techniques are also issues that must be addressed in the practical application of CGA electrochemical sensors. Furthermore, to better understand the development of electrochemical CGA sensors, a clear understanding of the physicochemical and electronic interactions occurring at the interface between nanomaterials and target analytes is needed. However, current research on the mechanism of structure–activity relationships between nanostructures and electrochemical analytical performance is relatively sparse. This lack of theoretical support might lead to inaccurate attributions of sensor performance. Most research is limited to focusing only on the number of electron transfers (this value is usually obtained through approximate calculations and is generally considered to be a two-electron, two-proton reaction) involved in the redox reaction of CGA on electrode materials, without considering the role of the electrode material in the system. Typically, studies assume that the electrode material plays a catalytic role in electrochemical detection, but in reality, there is little research on the catalytic reaction mechanism. For instance, techniques such as mass spectrometry and infrared spectroscopy are rarely used to study the intermediate species in catalytic reactions, which can reveal the specific steps and mechanisms of the catalytic process.

Moreover, theoretical calculations are useful tools for mechanism studies, linking theory with experiments can clarify the mechanisms of catalytic reactions clearer. Therefore, it is necessary to consider using more advanced characterization techniques for *in situ* observation and characterization of electrode surface reactions.

Looking ahead, to foster the practical application of electrochemical sensors for CGA analysis, the design of portable electrochemical sensors suitable for on-site detection is expected to become a major research focus. With the advent of the Internet of Things and the proliferation of portable devices, constructing portable electrochemical sensing platforms that can be operated *via* smartphones is anticipated to be a key area of innovation. These portable sensors will need to exhibit rapid response times, ease of operation, and high reliability to meet the demands of real-world applications.

Data availability

No primary research results, software or code have been included and no new data were generated or analysed as part of this review.

Conflicts of interest

There are no conflicts to declare.

Acknowledgements

We acknowledge the funding support from the Anhui University of Chinese Medicine Foundation (No. 2022rcZD006), National Natural Science Foundation of China (22301267).

References

1 V. Raskar and M. R. Bhalekar, *J. Drug Delivery Ther.*, 2019, **9**, 477.
2 M. Plazas, J. Prohens, A. N. Cuñat, S. Vilanova, P. Gramazio, F. J. Herraiz and I. Andújar, *Int. J. Mol. Sci.*, 2014, **15**, 17221.
3 S. F. Nabavi, S. Tejada, W. N. Setzer, O. Gortzi, A. Sureda, N. Braidy, M. Daglia, A. Manayi and S. M. Nabavi, *Curr. Neuropharmacol.*, 2017, **15**, 471.
4 T. Tsuchiya, O. Suzuki and K. Igarashi, *Biosci., Biotechnol., Biochem.*, 1996, **60**, 765.
5 M. D. dos Santos, M. C. Almeida, N. P. Lopes and G. E. de Souza, *Biol. Pharm. Bull.*, 2006, **29**, 2236.
6 K. L. Johnston, M. N. Clifford and L. M. Morgan, *Am. J. Clin. Nutr.*, 2003, **78**, 728.
7 E. Thom, *Int. J. Med. Res.*, 2007, **35**, 900.
8 S. H. Kwon, H. K. Lee, J. A. Kim, S. I. Hong, H. C. Kim, T. H. Jo, Y. I. Park, C. K. Lee, Y. B. Kim, S. Y. Lee and C. G. Jang, *Eur. J. Pharmacol.*, 2010, **649**, 210.
9 P. A. Lapchak, *Exp. Neurol.*, 2007, **205**, 407.
10 A. Suzuki, D. Kagawa, R. Ochiai, I. Tokimitsu and I. Saito, *Hypertens. Res.*, 2002, **25**, 99.
11 A. Suzuki, A. Fujii, N. Yamamoto, M. Yamamoto, H. Ohminami, A. Kameyama, Y. Shibuya, Y. Nishizawa, I. Tokimitsu and I. Saito, *FEBS Lett.*, 2006, **580**, 2317.
12 I. Onakpoya, R. Terry and E. Ernst, *Gastroenterol. Res. Pract.*, 2011, **2011**, 382852.
13 M. Chao and X. Ma, *J. Food Drug Anal.*, 2014, **22**, 512.
14 S. R. Wildermuth, E. E. Young and L. M. Were, *Compr. Rev. Food Sci. Food Saf.*, 2016, **15**, 829.
15 G. Kendir, A. Güvenç and E. Dinç, *Planta Med.*, 2011, **77**, PA36.
16 Y. K. Chen, X. C. Liu, J. G. Li, G. D. Liu, Y. Guo, L. Cheng and Y. M. Wang, *Hepatobiliary Pancreatic Dis. Int.*, 2012, **11**, 148.
17 Q. Hu, W. Wang, Z. Q. Yang, L. Xiao, X. Gong, L. Liu and J. Han, *Food Chem.*, 2023, **404**, 134395.
18 H. Yang, L. Yang, Y. Yuan, S. Pan, J. Yang, J. Yan, H. Zhang, Q. Sun and X. Hu, *Spectrochim. Acta, Part A*, 2018, **189**, 139.
19 L. M. Magalhaes, S. Machado, M. A. Segundo, J. A. Lopes and R. N. Pascoa, *Talanta*, 2016, **147**, 460.
20 Z. Li, D. Huang, Z. Tang, C. Deng and X. Zhang, *Talanta*, 2010, **82**, 1181.
21 I. G. Munteanu and C. Apetrei, *Int. J. Mol. Sci.*, 2021, **22**, 13138.
22 J. Baranwal, B. Barse, G. Gatto, G. Broncova and A. Kumar, *Chemosensors*, 2022, **10**, 363.
23 A. Lochab, S. Baxi, P. Tiwari, S. Bardiya and R. Saxena, *Microchem. J.*, 2024, **199**, 109923.
24 M. Mehmandoust, M. Soylak and N. Erk, *Talanta*, 2023, **253**, 123991.
25 K. Y. Goud, M. Satyanarayana, A. Hayat, K. V. Gobi and J. L. Marty, in *Nanoparticles in Pharmacotherapy*, Elsevier, 2019, pp. 195.
26 A. K. Srivastava, S. S. Upadhyay, C. R. Rawool, N. S. Punde and A. S. Rajpurohit, *Curr. Anal. Chem.*, 2019, **15**, 249.
27 A. J. Bard, L. R. Faulkner and H. S. White, *Electrochemical methods: fundamentals and applications*, John Wiley & Sons, 2022.
28 C. Forzato, V. Vida and F. Berti, *Biosensors*, 2020, **10**, 105.
29 M. N. Islam and R. B. Channon, in *Bioengineering Innovative Solutions for Cancer*, ed. S. Ladame and J. Y. H. Chang, Academic Press, 2020, pp. 47.
30 C. Zhu, G. Yang, H. Li, D. Du and Y. Lin, *Anal. Chem.*, 2015, **87**, 230.
31 N. Jadon, R. Jain, S. Sharma and K. Singh, *Talanta*, 2016, **161**, 894.
32 J. Wang, S. Pan, W. Sun and Y. Wang, *New J. Chem.*, 2024, **48**, 1792.
33 T. Zhao, X. Niu, W. Y. Pei and J. F. Ma, *Anal. Chim. Acta*, 2023, **1276**, 341653.
34 Y. Yang, P. Wang, Z. Luo, J. Li, Y. Wang, Z. Li, C. Chen, Y. Xie, P. Zhao and J. Fei, *Chem. Eng. J.*, 2023, **468**, 143815.
35 E. Beyyavas and M. Aslanoglu, *Food Chem.*, 2023, **426**, 136600.

36 V. Mariyappan, S.-M. Chen, T. Jeyapragasam and J. M. Devi, *J. Alloys Compd.*, 2022, **898**, 163028.
37 W. Li, X. Deng, Z. Wu, L. Zhang and J. Jiao, *ACS Omega*, 2022, **7**, 4614.
38 A. J. Jesu Amalraj and S.-F. Wang, *Mater. Today Chem.*, 2022, **26**, 101154.
39 Y. Yan, X. Bo and L. Guo, *Talanta*, 2020, **218**, 121123.
40 T. Teker and M. Aslanoglu, *Arabian J. Chem.*, 2020, **13**, 5517.
41 X. Zhao, J. Bai, X. Bo and L. Guo, *Anal. Chim. Acta*, 2019, **1075**, 71.
42 K. Manivannan, M. Sivakumar, C.-C. Cheng, C.-H. Lu and J.-K. Chen, *Sens. Actuators, B*, 2019, **301**, 127002.
43 R. Chokkareddy, G. G. Redhi and T. Karthick, *Heliyon*, 2019, **5**, e01457.
44 Y. Chen, W. Huang, K. Chen, T. Zhang, Y. Wang and J. Wang, *Talanta*, 2019, **196**, 85.
45 T. Zhang, Y. Chen, W. Huang, Y. Wang and X. Hu, *Sens. Actuators, B*, 2018, **276**, 362.
46 A. Yiğit, N. Alpar, Y. Yardım, M. Çelebi and Z. Şentürk, *Electroanalysis*, 2018, **30**, 2011.
47 T. Zhang, M. Liu, Q. Zhang, Y. Wang, X. Kong, L. Wang, H. Wang and Y. Zhang, *Analyst*, 2017, **142**, 2603.
48 W. Cheng, J. Huang, C. Liu, Q. Zeng, Y. Tong, L. Wang and F. Cheng, *RSC Adv.*, 2017, **7**, 6950.
49 Y. Wang, H. Chen, X. Hu and H. Yu, *Analyst*, 2016, **141**, 4647.
50 C. M. Ribeiro, E. M. Miguel, J. D. S. Silva, C. B. D. Silva, M. O. F. Goulart, L. T. Kubota, F. B. Gonzaga, W. J. R. Santos and P. R. Lima, *Talanta*, 2016, **156–157**, 119.
51 J. Ganesamurthi, R. Shanmugam, S.-M. Chen, K. Alagumalai, M. Balamurugan and Y.-Y. Yu, *Mater. Chem. Phys.*, 2022, **292**, 126757.
52 W. Jiang, Z. Zhuo, X. Zhang, H. Luo, L. He, Y. Yang, Y. Wen, Z. Huang and P. Wang, *Food Chem.*, 2024, **431**, 137165.
53 I. G. Munteanu and C. Apetrei, *Int. J. Mol. Sci.*, 2021, **22**, 8897.
54 X. Ma, Y. Gao, W. Pang, X. Chang, Z. Hu and T. Hu, *J. Electroanal. Chem.*, 2024, **961**, 118235.
55 J. Jency Feminus and P. N. Deepa, *Mater. Chem. Phys.*, 2022, **289**, 126440.
56 N. Mohammadi, M. Najafi and N. B. Adeh, *Sens. Actuators, B*, 2017, **243**, 838.
57 M. Liao, Y. Yang, J. Ou, H. Yang, X. Dai, L. Zhong and L. Wang, *Electrochem. Commun.*, 2024, **165**, 107754.
58 L. S. Porto, D. N. Silva, A. E. F. de Oliveira, A. C. Pereira and K. B. Borges, *Rev. Anal. Chem.*, 2019, **38**, 20190017.
59 N. L. Teradal and R. Jelinek, *Adv. Healthc. Mater.*, 2017, **6**, 1700574.
60 E. M. Kirchner and T. Hirsch, *Mikrochim. Acta*, 2020, **187**, 441.
61 S. K. Kaiser, Z. Chen, D. Faust Akl, S. Mitchell and J. Pérez-Ramírez, *Chem. Rev.*, 2020, **120**, 11703.
62 M. Mehmandoust, G. Li and N. Erk, *Ind. Eng. Chem. Res.*, 2022, **62**, 4628.
63 S. J. Malode, M. M. Shanbhag, R. Kumari, D. S. Dkhar, P. Chandra and N. P. Shetti, *J. Pharm. Biomed. Anal.*, 2023, **222**, 115102.
64 M. Pumera, *Chem. Soc. Rev.*, 2010, **39**, 4146.
65 M. Donarelli and L. Ottaviano, *Sensors*, 2018, **18**, 3638.
66 H. Meskher, T. Ragdi, A. K. Thakur, S. Ha, I. Khelfaoui, R. Sathyamurthy, S. W. Sharshir, A. K. Pandey, R. Saidur, P. Singh, F. Sharifian Jazi and I. Lynch, *Crit. Rev. Anal. Chem.*, 2023, 1, DOI: **10.1080/10408347.2023.2171277**.
67 Z. Wen, S. Ci, Y. Hou and J. Chen, *Angew. Chem., Int. Ed.*, 2014, **53**, 6496.
68 L. Lu, J. Liu, Y. Hu, Y. Zhang, H. Randriamahazaka and W. Chen, *Adv. Mater.*, 2012, **24**, 4317.
69 K. Tian, Y. Ma, Y. Liu, M. Wang, C. Guo, L. He, Y. Song, Z. Zhang and M. Du, *Sens. Actuators, B*, 2020, **303**, 127199.
70 N. Stock and S. Biswas, *Chem. Rev.*, 2012, **112**, 933.
71 C.-S. Liu, J. Li and H. Pang, *Coord. Chem. Rev.*, 2020, **410**, 213222.
72 T. Ma, H. Li, J. G. Ma and P. Cheng, *Dalton Trans.*, 2020, **49**, 17121.
73 B. Yuan, W. Xing, Y. Hu, X. Mu, J. Wang, Q. Tai, G. Li, L. Liu, K. M. Liew and Y. Hu, *Carbon*, 2016, **101**, 152.
74 J. Duan, S. Chen, M. Jaroniec and S. Z. Qiao, *ACS Catal.*, 2015, **5**, 5207.
75 H. Mei, Y. Mei, S. Zhang, Z. Xiao, B. Xu, H. Zhang, L. Fan, Z. Huang, W. Kang and D. Sun, *Inorg. Chem.*, 2018, **57**, 10953.
76 J. Li, X. Li, Z. Yin, X. Wang, H. Ma and L. Wang, *ACS Appl. Mater. Interfaces*, 2019, **11**, 29004.
77 Y. Wang, Z. Nie, X. Li, R. Wang, Y. Zhao and H. Wang, *ACS Sustainable Chem. Eng.*, 2022, **10**, 6082.